Materials Advances

Accepted Manuscript

This article can be cited before page numbers have been issued, to do this please use: C. Lee, S. Leguizamon, M. Tetzloff, D. Rudykh, B. Jones, O. Davydovich, D. J. Hayne, L. C. Henderson and A. Boydston, *Mater. Adv.*, 2026, DOI: 10.1039/D5MA01441G.

View Article Online
DOI: 10.1039/D5MA01441G

Additive Manufacturing of Poly(dicyclopentadiene) and Carbon-Fiber Composites via Heating at a Patterned Photothermal Interface

Chang-Uk Lee[a]; Samuel C. Leguizamon[b,c]; Brad H. Jones[b]; Oleg Davydovich[b]; David Hayne[d]; Margaret E. Tetzloff[a]; Daria Rudykh[a]; Luke Henderson[d]; AJ Boydston[a,e,f*]

[a]Department of Chemistry, University of Wisconsin, Madison, Wisconsin 53706, USA

[b]Sandia National Laboratories, Albuquerque, New Mexico, 87185, USA

[c]Biodesign Center for Sustainable Macromolecular Materials and Manufacturing (SM3), Arizona State University, Tempe, Arizona, 85281, USA

[d]Institute for Frontier Materials, Deakin University, Geelong, Victoria 3220, Australia

[e]Department of Chemical & Biological Engineering, University of Wisconsin, Madison, Wisconsin 53706, USA

[f]Department of Materials Science & Engineering, University of Wisconsin, Madison, Wisconsin 53706, USA

ABSTRACT

We report vat-type additive manufacturing (AM) of poly(dicyclopentadiene) (pDCPD) and carbon-fiber (CF) composites via heating at a patterned photothermal interface (HAPPI) by using thermo-responsive polysulfone (PSU)-encapsulated Hoveyda-Grubbs second generation catalyst (HG2) polymer microparticles (PSU-HG2 PMPs). Photothermal conversion of light to thermal energy in HAPPI enabled the release of HG2 in the resin followed by localized thermal curing according to the dictated light pattern. Complex structures of pDCPD were generated by controlling the amount of the catalyst microparticles, print conditions (temperature, speed, and layer thickness), and aging time for the resin mixture prior to AM. In addition to pDCPD parts, AM of pDCPD-CF composites was also enabled by HAPPI and facilitated by the fact that HAPPI AM does not impose limits on the optical properties of the resin. We describe the mechanical performance of pDCPD and composite specimens produced via HAPPI AM, and present microstructural studies from scanning electron microscopy (SEM) and CT analyses. HAPPI AM is demonstrated as a useful tool to create complex three-dimensional (3D) structures of pDCPD and tensile test specimens of pDCPD-CF composites from vat-like AM.

1. Introduction

Poly(dicyclopentadiene) (pDCPD) prepared by ring opening metathesis polymerization (ROMP) is recognized as one of the most attractive thermoset resins in industry and academia. It displays high notch-impact strength, high temperature and corrosion resistance properties, excellent stability against chemicals, and can manifest relatively polar surfaces after quick oxidation in air that makes it compatible with various coatings.[1,2] Materials based on pDCPD or reinforced pDCPD composites are used for manufacturing of agriculture equipment, heavy-vehicle panels, and electrolyte cell coverings.[1,3,4] Usually, pDCPD is processed by reaction injection molding, resin transfer molding (RTM), and vacuum-assisted RTM.[1] Those methods limit the structures and shapes of pDCPD products due to the rapid polymerization with highly

View Article Online
DOI: 10.1039/D5MA01441G

active transition metal catalysts.[4] Additive manufacturing (AM), also referred to as 3D printing (3DP), has emerged as an alternative solution to create pDCPD parts with complex architectures thanks to breakthroughs in photoinitiated ROMP and the development of latent catalysts that increase the pot life of DCPD based resins.[3,5–7] For example, Leguizamon et al.[8] reported direct ink writing (DIW) AM and stereolithographic AM of pDCPD by employing photosensitizers and thermally latent catalyst systems. Prior to their work, PolySpectra, Inc. and Promerus each disclosed commercial variants of photomediated ROMP AM with resins that display long-term stability and produce parts with tunable mechanical properties.[9,10]

Frontal ROMP (FROMP) involves initial exothermic reactions that are usually initiated by light or heat and then induce a propagating polymerization front through a resin with high energy density.[11–13] FROMP has been established as an inspiring approach to produce high-performance pDCPD thermosets despite the finite pot life of DCPD resin. Often, spontaneous polymerization of highly reactive monomers such as DCPD with widely used ruthenium metathesis catalysts presents significant challenges for achieving controlled FROMP.[3,14,15] To extend the pot life of DCPD resin mixtures and to prevent spontaneous polymerization, it has been advantageous to control ROMP chemistry by adding a chain transfer agent such as limonene; ROMP inhibitors such as triphenylphosphine, *N,N*-dimethylaminopyridine, and alkyl phosphites; or employing thermally latent catalysts such as bis-*N*-heterocyclic carbene complexes.[11] Alternatively, Leguizamon et al.[3] reported polysulfone (PSU)-encapsulated Hoveyda-Grubbs second generation catalyst (HG2) polymer microparticles (PSU-HG2 PMPs) to extend the storage life of DCPD and HG2 formulations to greater than 12 months. In the microparticles, HG2 is locally separated from DCPD by PSU encapsulation, and the PSU barrier can be compromised by increasing the temperature of the PSU-HG2 PMPs above ca. 60 ˚C.

Recently, Lee et al. developed a new AM method termed heating at a patterned photothermal interface (HAPPI).[16–18] The HAPPI AM system (Fig. 1 A, B) was designed such that a photothermal vat is used to achieve AM of legacy thermosets such as Pt-cured silicones, urethanes, or epoxies that are commonly used in molding processes and have typically required chemical modification to allow for AM by light-based technologies like vat photopolymerization (VP). In HAPPI AM, light is still projected to dictate the sequential 2D patterns that represent individual layers of a 3D part (that is preserved between HAPPI and conventional VP). However, instead of using the projected light to drive a photochemical initiation within the resin, the light is converted to heat at the interface of the resin and bottom of the vat. Specifically, we use a photothermal plate as the bottom of the vat, which can reach temperatures exceeding 200 °C almost instantaneously upon exposure to near-infrared (near-IR) light. The patterned light (or laser rastering) dictates the pattern of heat on the bottom of the vat, which is then translated into a thermally cured resin layer. Mechanizing the process into a sequential layer-by-layer sequence achieves 3D parts without requiring any new chemistry in the resin components (i.e., they are thermally cured as they would be in a molding process). During AM, each layer of the thermoset resin is solidified onto the preceding layer through thermal curing that is driven by the patterned heat generated at the photothermal plate. HAPPI was used to demonstrate AM of thermosets

View Article Online
DOI: 10.1039/D5MA01441G

such as Pt-cured silicones and thermally denatured proteins without requiring any chemical modifications to the build materials while resolutions are limited to millimeter scale.[16–18] Notably, since the optical properties of the resin are irrelevant, we envisioned that HAPPI may be well-suited for AM of filled materials to produce composites that would otherwise impose challenges to VP AM techniques. Combinations of DCPD and CF in AM have been reported mostly via direct ink write (DIW) AM of composites composed of discontinuous CF and DCPD via FROMP using Grubbs-type II catalysts.[19–27] For example, Zhang et al.[26] reported DIW AM of composites composed of discontinuous CF and DCPD via FROMP using Grubbs-type II catalysts. DIW may require the heated build plate,[14,20,21] in-situ photothermal curing,[22] or photothermal initiation.[19,28] Dojan et al.[22] reported AM of composites of discontinuous or continuous CFs via remote photothermal heating of CF using the blue laser beam (wavelength = 450 m). Hmeidat et al.[27] demonstrated AM of CF-reinforced polymer (CFRP) composites composed of pDCPD and continuous CFs via frontal polymerization (FP)-DIW process including extrusion, compaction and in-situ curing. With a such DIW approach, building 3D structures along the Z axis would be challenging once FROMP occurs, which may account for why products with complex structures including internal voids were rarely reported.

In contrast to DIW, vat-type AM technologies are rare in combination with DCPD and CF due to the optical challenges imposed by the CF though they offer benefits of excellent geometric freedom and are efficient for producing complex structures. There are recent reports on progress in VP of fiber reinforced polymeric composites while challenges to achieve 3D structures with high loading of fiber additives are still remaining. Asif et al.[29] reported VP of photocurable resin with CFs up to 4 % w/v, but only single layers of dogbones were reported. Wang et al.[30] reported VP of ceramic slurry mixed with photocurable resin with CFs up to 0.3 wt% due to optical limits of the resin. Lu et al.[31] reported VP of resin and continuous fibers, but resin curing was separated from fiber loading. In this study, we took advantage of HAPPI as one of the vat-type technologies with geometric freedom and no limits in optical properties of resin for high loading of additives. Combined with the PSU-HG2 PMPs as thermo-responsive catalyst particles and appropriate CF additives, we demonstrate AM of pDCPD and pDCPD-CF composite parts via HAPPI and evaluation of their mechanical performance.

View Article Online
DOI: 10.1039/D5MA01441G

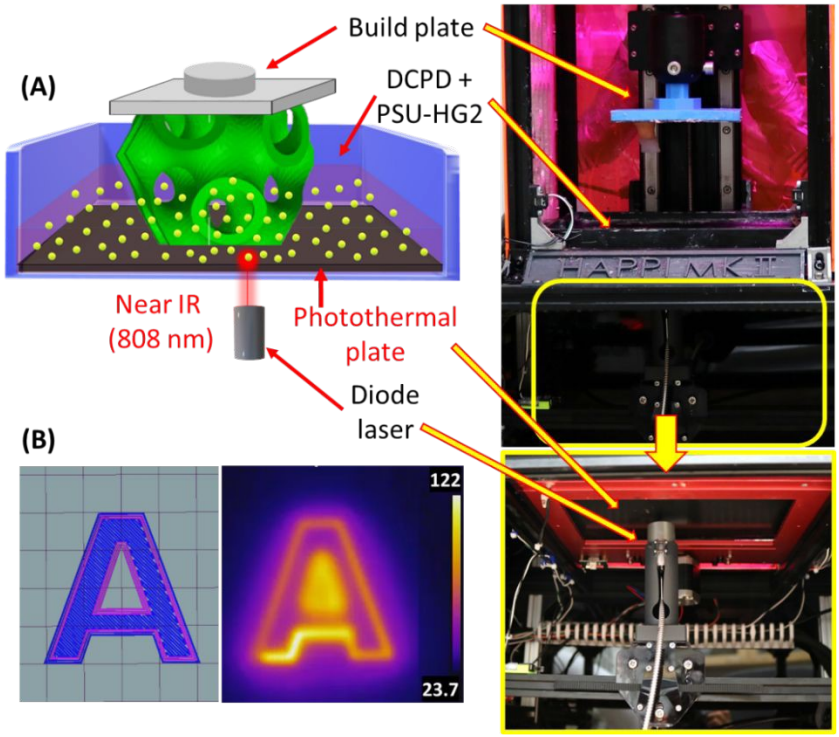

Fig. 1 (A) Generalized schematic for HAPPI AM of DCPD with PMPs, (B) (left) letter "A" CAD model and photothermal image showing the temperature evolution during printing.

2. Experimental

2.1 Materials

Dicyclopentadiene (DCPD) and 5-ethylidene-2-norbornene (ENB) were purchased from Sigma-Aldrich and used as received. PSU-HG2 PMPs were prepared by a previously reported method.[3] PMPs were prepared using an oil-in-water emulsion solvent evaporation technique. Aqueous phase was prepared by vigorous mixing of 0.19 g poly(ethylene-alt-maleic anhydride) in 5 mL water until fully dissolved. Oil phase was prepared by first dissolving 0.125 g of the encapsulating polymer (PSU) in 1.4 mL dichloromethane (DCM). Each solution was vigorously mixed at room temperature until fully homogenized. Directly prior to emulsification, 17.5 mg of catalyst (HG2) was added to the DCM solution and gently stirred. The oil phase was transferred to a vial containing the aqueous phase. Then, a VWR 200 homogenizer was inserted and operated at medium speed for 90 s to emulsify the given sample. A magnetic stir bar was then added to each emulsion and the DCM allowed to evaporate in air overnight with the stir bar rotation speed set at 1000 RPM. Upon removal of the DCM, the dispersion was transferred into a pre-weighed, 15 mL impact-resistant centrifuge tube, then diluted with water until it reached 15 mL total volume. The solution was centrifuged down, decanted, filled with fresh DI water, and redispersed. This process was repeated two times to remove as much poly(ethylene-alt-maleic anhydride) as possible. To the last decanted mixture was added 0.5 to 2 mL of DI water. Each dispersion was suspended in liquid nitrogen then freeze dried to remove all water. Pitch-based Dialead™ milled CF (200 μm avg. length) was sourced from Mitsubishi Chemical Corporation

View Article Online
DOI: 10.1039/D5MA01441G

(Japan). Norbornene-functionalized CF (fCF) was prepared by a previously reported method.[32] A typical modification process is given here: a round bottom flask containing 1 M HCl was cooled to 0 °C, and a hydrochloride salt of the pentyl aniline derivate (810 mg, 3.75 mmol) and norbornene aniline derivative (664 mg, 1.87 mmol) was added dropwise in DMF (1 mL) to give 2:1 M ratio of anilines, respectively. The mixture was left stirring and left to gradually warm to ambient temperature. After 2 h, milled CF was added, and the mixture was heated to reflux for 24 h. The milled CF was isolated by vacuum filtration, and washed with deionized water, methanol, ethanol, chloroform, and dichloromethane before being dried at the pump. Linear oligoDCPD (M_n = 2.4 kDa) was sourced from Boydston Chemical Innovation, Inc. (BCI). Poly(tetracyclododecene)-imide-norbornene (pTD-NB) was prepared by the procedure described in the Supporting Information (Figs. S1-S9).

2.2 Resin formulations and HAPPI AM

PSU-HG2 PMPs at 0.4 wt% were vigorously stirred in DCPD/ENB (95/5 weight ratio) at room temperature for 4 to 7 days to create a uniform suspension. For composites, CF or fCF at 5 or 10 wt% were stirred in the PMPs/DCPD mixture for 4 to 7 days. The CF in DCPD appeared visually to be well-dispersed throughout the resin almost immediately upon mixing. The resin formulations containing particles were aged according to our differential scanning calorimetry (DSC) analyses. Small batch variations and shelf-life differences can result in slightly different onset temperatures for curing, which can be addressed by aging the samples and assessing the onset curing temperature via DSC. In our experiments, we found that aging for 4 to 7 days, during which time DSC analyses were conducted intermittently, was ideal. The ideal time that was used for mixing these materials was dependent on the onset temperature in the DSC traces. For more detailed information on particle aging and activity, we refer to the previous work describing improved catalyst release from particles after prolonged stirring.[3] We used the previously reported HAPPI setup where two major components are assembled: (1) a diode laser mounted on a modified gantry system from a laser engraver and (2) a z-axis assembly including stepper motor and linear rails taken from a commercial digital light processing (DLP) 3D printer.[16–18] We used a diode laser with a wavelength of 808 nm that was purchased from Opto Engine LLC (Midvale, UT, USA). Repetier-Host was used to load STL files, slice models, and execute the printing. The STL files were converted to G-code files using Prusa slicer. STL files of gyroid, spiral, or ASTM D638-IV dogbones were obtained from open sources, GrabCAD or Thingiverse. In some cases, STL files were further modified by using Prusa slicer or Tinkercad. The infill pattern was a line at 95% density. The laser light was directed through a fiber optic cable with a diameter of 550 μm and a collimator with a beam diameter of 5 mm. The major print speed was 3,000 to 3,600 mm·min^{-1} for dogbones and 2,400 mm·min^{-1} for gyroids. Layer thickness was set to be 0.3 mm. Temperatures of the grill mat were monitored by thermal IR camera (Topdon, TC005) on the same side as the laser. During printing, the temperature reading was maintained between 150 to 200 ˚C by controlling laser intensity, laser travel speed (i.e., print speed), or both. Printed dogbones were post-cured in an oven at 150 ˚C for 3 hrs. For molded

View Article Online
DOI: 10.1039/D5MA01441G

samples, PSU-HG2 PMPs at 0.4 wt% were vigorously stirred in DCPD/ENB at room temperature for 14 days. The mixture was poured into PTFE dogbone molds (modified ASTM D638-IV: 20 % wider, central gauge region than the standard). FROMP was initiated by heating the edge of the dogbone mold for 10 seconds using a soldering iron (nominally 80 W, purchased from Amazon.com) set at 180 ˚C. Molded dogbones were post-cured in an oven at 150 ˚C for 3 hrs.

The open bottom of the vat was covered by a black PTFE grill mat (0.2 mm thickness, purchased from Amazon.com), which was used as a photothermal plate. The diode laser was pointed toward the PTFE mat while its movement was dictated by G-code. The PTFE mat converts light to heat, leading to release of the HG2 catalyst from the PMPs followed by curing of the DCPD. To identify suitable photothermal materials, we looked at the temperature profiles of seven materials that were commercially available as thin black sheets, each illuminated with an 808-nm laser.[16] The materials included polycarbonate, acrylic, steel, silicone, and PTFE of various thicknesses. Important metrics were the cure time for a thin layer of thermoset resin (e.g., Sylgard 184 silicone), the size of a localized heating area, and time to cool down after curing. The localized heating area from the plastic plates was found to be much smaller than that from the steel plate, likely due to higher thermal conductivity (250-fold) and thermal diffusivity (80-fold) of the steel plates. Among the plastic plates of similar thermal conductivities, the thinner (0.1- or 0.2-mm thickness) PTFE sheets showed smaller heating areas, as well as higher rates of heating and cooling, than thicker ones (1.0- or 1.5-mm thickness). Additionally, PTFE showed low surface adhesion of the cured resin. The PTFE mat, composed of woven glass fiber with black PTFE coating, showed promising thermal stability and mechanical durability during multiple curing cycles compared to the other plates.

2.3 Instruments

Uniaxial tensile testing was conducted using the Material Testing System (MTS, Eden Prairie, MN, USA) Criterion Model 43 with a 50 kN load cell at an extension rate of 2 $mm \cdot min^{-1}$. Modified ASTM D638 type IV (20 % wider gauge region than standard) samples for tensile testing were prepared by HAPPI AM. Differential scanning calorimetry (DSC) studies were conducted on a TA DSC Q200 calorimeter under nitrogen. Mixtures of DCPD with 0.4 wt% PSU-HG2 or DCPD with 0.4 wt% PSU-HG2 and10 wt% CF were sealed in an aluminum pan with a hermetic lid, and heat flow was recorded while heating at 10 $˚C \cdot min^{-1}$.

Rheological measurements on DCPD with 0.4 wt% PMPs without or with CFs after stirring for 2 hrs or 5 days were performed using a Discovery HR 20 rheometer (TA Instruments) at 21 ºC with a 60 mm parallel plate and a gap of 0.5 mm. Apparent viscosities were obtained through a logarithmic shear-rate sweep from 0.1 s^{-1} to 100 s^{-1}. Dynamic mechanical analyses (DMA) on rectangles of pDCPD or pDCPD with CFs were done on a PerkinElmer DMA 8000. Sinusoidal forces were applied to rectangular samples within linear viscoelastic regions (strain = 0.05) at a constant frequency (1 Hz) as a function of temperature. Temperature ranges for analyses were 27 to 220 °C, and the heating rate was 2 °C min^{-1} for all samples. Logarithmic

View Article Online
DOI: 10.1039/D5MA01441G

values of storage modulus (E') of the samples as well as tan (δ) were reported as a function of temperature. SEM imaging on the fractured dogbone samples after tensile tests was conducted using a Zeiss Gemini SEM 450 at an accelerating voltage of 5 kV. SEM samples were sputter-coated with 5-nm thick gold. X-Ray micro-computed tomography (CT) was performed using a Rigaku CT Lab HX 130 benchtop instrument from Rigaku Americas Corporation (The Woodlands, TX, USA). The specimens were imaged using a traditional X-ray micro source with a W anode operated at 70 kV applied voltage and 114 µA applied current. For the larger gyroid and spiral structures, the sample-to-source distance was 33 cm, whereas for the dogbone specimens, a small portion of the gauge region near the fracture surface after tensile tests was imaged with a sample-to-source distance of 4.7 cm. These imaging conditions yielded a voxel size of 37.4 µm and 5.3 µm, respectively. Two-dimensional (2D) images were collected in a continuous scan mode while rotating the specimens through 360° over 68 min total scan time. The 2D images were center-corrected and used to generate a 3D reconstruction of the specimen. Gel fraction and equilibrium swelling ratio of printed samples were measured by swelling in ethanol, which is good solvent for DCPD, and using the following formula:[33]

Gel fraction (%) = $(W_2/W_0)\times100$

Equilibrium swelling ratio (%) = $((W_1-W_0)/W_0)\times100$

W_0: weight of dried sample, W_1: weight of the sample after swelling in ethanol, W_2: weight of dried sample after measuring W_1.

3. Results and discussion

3.1 HAPPI AM of pDCPD and pDCPD-CF composites

Fig. 2(A) shows a generalized schematic of the HAPPI design that depicts thermal activation of PMPs within a DCPD resin. Fig. 2(B) shows the generalized olefin metathesis polymerization reactions of DCPD as well as a depiction of the final network structure of crosslinked pDCPD. During HAPPI AM, localized heating is generated by rastering a near-IR laser along chosen design patterns on the bottom of the photothermal plate. Whereas Leguizamon and co-workers' report was designed to induce FROMP throughout the entire volume of the resin,[3] HAPPI AM requires that only localized heating take place, at the exclusion of a runaway propagating polymerization front, and therefore it was critical that we controlled the reactivity of the PMPs during HAPPI AM. The onset temperature for activation was evaluated first by DSC. Fig. S10 and Fig. S11 shows DSC thermograms of DCPD with PMPs without or with 10 wt% CFs after stirring for 2 hrs or 4 days, respectively. For DCPD, we observed an irrersible, exothermic peak at 96 ˚C (enthalpy of curing = 76 J/g) with an onset temperature at 93 ˚C after stirring 2 hrs, and a peak at 95 ˚C (enthalpy of curing = 90 J/g) with an onset at 87 ˚C after stirring for 4 days. For DCPD with CFs, we observed an irrersible, exothermic peak at 98 ˚C (enthalpy of curing = 136 J/g) with an onset temperature at 91 ˚C after stirring 2 hrs, and two peaks at 90 and 97 ˚C (enthalpy of curing = 99 J/g) with an onset at 85 ˚C after stirring for 4 days. For both DCPD and DCPD with CFs, the onset temperature for curing decreased by 5 or 6˚ after stirring 4 days (Table S1). Those exothermic peaks were not observed in the printed samples, indicating complete curing

View Article Online
DOI: 10.1039/D5MA01441G

during HAPPI, and with no peaks observed after post-curing (Fig. S12). Additionally, we studied any impact of aging on viscosity and curing activities of the resin by rheology. Figs. S13 and S14 show apparent viscosities of DCPD with 0.4 wt% PMPs without or with 10 wt% CFs after stirring for 2 hrs and 5 days in the range of shear rate from 1 to 100 s^{-1}, respectively. The viscosities of DCPD remain almost identical (around 5 mPa·s) after stirring 5 days. The viscosities of of DCPD with CFs ranged from 10 to 18 mPa·s after stirring 2 hrs, and increased to the range from 68 to 98 mPa·s after stirring 5 days at low shear rate (1 to 10 s^{-1}). In this case, we consider that the PMPs would be more activated in the presence of CFs though we need more studies on them. DSC and rheological studies show aging for less than 7 days did not affect the stabitliy of the resin, but facilitated curing during HAPPI printing.

Above the onset temperature, the HG2 catalyst is released from the encapsulated PMPs and the resin is crosslinked via ROMP. Then, following several empirical observations, we arrived at generalized formulations and printing parameters for HAPPI AM of DCPD and DCPD with CF. Specifically, we reduced the concentration of PMPs from 0.8 to 0.4 wt%. We observed qualitatively that reducing the amount of PMPs to 0.4 wt% significantly delayed the initiation for FROMP in bulk molding experiments, which proved advantageous in avoiding full curing of the resin volume in HAPPI AM. The thickness of the layers in HAPPI was limited to 0.3 mm, thus limiting the ability of heat generated from the exothermic polymerization to propagate through the material in the z-direction. The PMPs were stirred in DCPD at room temperature for 4 to 7 days, since prolonged agigation is expected to reduce particle aggregation or directly break particles into smaller fragments.[3] Indeed, prior work demonstrated a decrease in average particle size from 3 to 2 μm for particles agitated over extended periods. During this period they observed a reduction in the breadth and onset temperature of exothermic cure peaks by DSC. Accordingly, we found that aging the mixture up to 7 days faciliated localized heating followed by localized curing during HAPPI AM while still providing parts with comparable mechanical properties to samples made via FROMP in molds. Aging for only 1 or 2 days resulted in printed parts with inferior mechanical properties. Aging for over 7 days resulted in a higher propensity to initiate FROMP of DCPD throughout the entire vat during HAPPI AM. Based on our empirical observations, we believe the catalyst particles exhibited slow release of the catalyst after aging for 1-2 days, and FROMP rarely occurred during printing. That may result in incomplete formation of network structures between norbornene and cyclopentene, leading to inferior mechanical properties. Once FROMP occurred in the resin with longer aging than 3 days, resulting in complete formation of network and excellent mechanical properties of pDCPD. Finally, the temperature measured at the photothermal plate outside of the vat was kept between 150 to 200 ˚C by controlling the laser raster speed and laser power to be between 3,000 to 3,600 mm·min^{-1} and via manual adjustments to the laser intensity during printing, which together minimized the evaporation of DCPD during HAPPI AM.

View Article Online
DOI: 10.1039/D5MA01441G

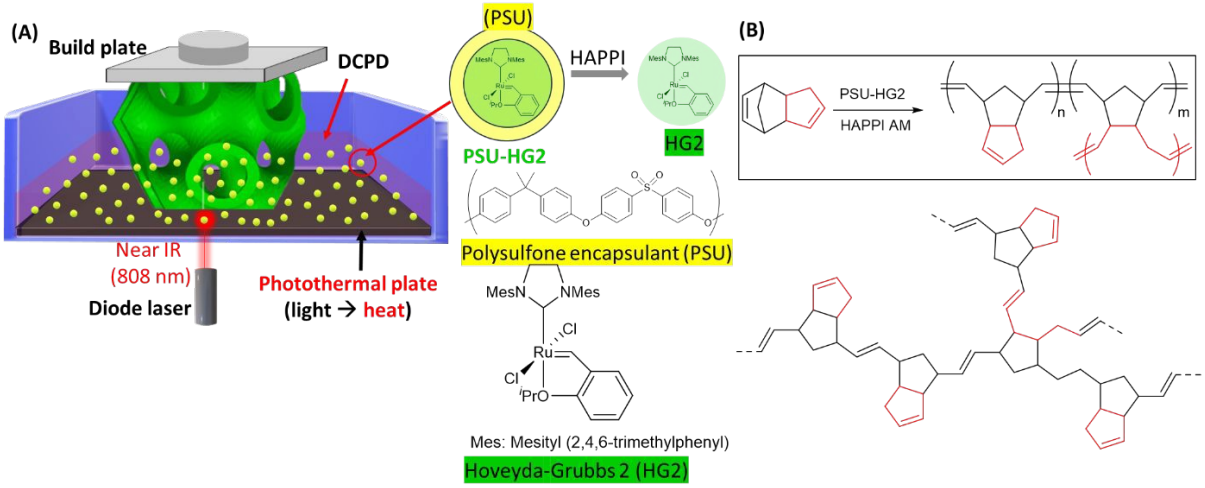

Fig. 2 Top: (A) A scheme for HAPPI design and PSU-HG2 catalyst particles and (B) a scheme of metathesis of reaction of norbornene and cyclopentene of DCPD with the network structures of crosslinked pDCPD.

To demonstrate AM of three dimensional pDCPD objects with complex structures, we prepared a spiral and gyroid via HAPPI AM without requiring any support structures during the process. The results in Fig. 3 show successful HAPPI AM of a spiral and gyroid on a relatively large scale (50 to 100 mm end-to-end distance) as well as their digital files for comparison. As can be seen, voids and overhangs were achieved without the need for support materials. Video compilations of CT-scans of the spiral and gyroid are presented in the Supporting Information (Figs. S21 and S22). These results show that localized photothermal heating and preclusion of runaway FROMP was successfully achieved by HAPPI with pDCPD and PMPs (originally designed for FROMP).

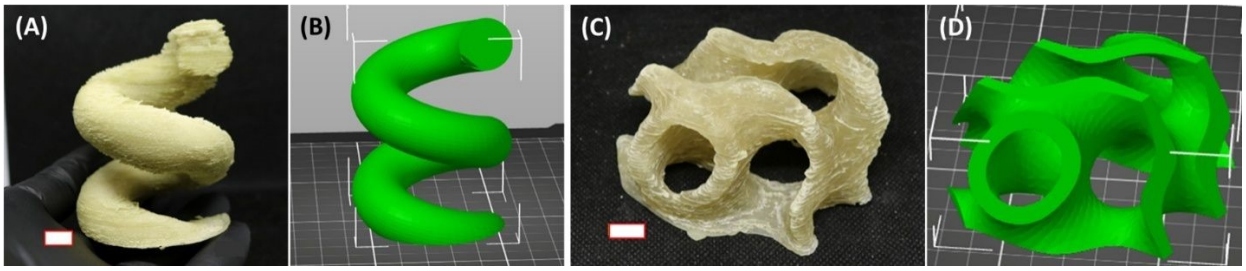

Fig. 3 HAPPI AM of pDCPD with PSU-HG2 PMPs as a thermos-responsive catalyst (A) a spiral, (B) digital file of spiral, (C) gyroid, and (D) digital file of gyroid (scale bar = 1 cm).

One of the advantages of HAPPI AM is that there are no limits on the optical properties of resin since HAPPI uses localized heating on a photothermal plate rather than photochemical activation within the resin. In contrast, most vat-type AM technologies that use light as an energy source rely on the optical transparency of resin. As a result, vat-type AM of filled or composite materials is often challenging. This is unfortunate considering that composites, such as those that

View Article Online
DOI: 10.1039/D5MA01441G

utilize CF, are of great utility in various applications. In AM studies, CF has been of great interest since CF displays the highest tensile modulus and tensile strength (from 210 to 240 GPa and 2,000 to 4,900 MPa, respectively) among synthetic fibers,[34] outstanding strength-to-weight ratio, negligible thermal expansion, and resistance to thermal and chemical environments.[35] As discussed in the introduction, combinations of DCPD and CF in AM have been reported mostly via DIW AM[19–28,36] that may require the heated build plate,[14,20,21] in-situ photothermal curing,[22] or photothermal initiation.[19,28] However, combinations of DCPD and CF in vat-type AM technologies providing excellent geometric freedom are rare due to the optical challenges imposed by the CF. In our study, we took advantage of HAPPI as one of the vat-type technologies to additively manufacture pDCPD composites with CF (pDCPD-CF). We incorporated pristine milled, 200-µm CF and fCF each at 5 and 10 wt% (giving sample types labeled as: pDCPD-5%CF, pDCPD-10%CF, pDCPD-5%fCF, or pDPCD-10%fCF) and included those in comparison with samples made from DCPD alone. In addition to the CFs, we further demonstrated two additional polymeric additives, linear oligoDCPD and poly(tetracyclododecene-*co*-norbornene), that can each be printed with DCPD via HAPPI 3DP. Since those exploratory additives did not enhance mechanical properties of the printed parts, we discontinued their study (see Fig. S15). We evaluated the gel fraction and equilibrium swelling ratio of parts in ethanol, which is good solvent for DCPD (Table 1). The gel fraction of each of the pDCPD and composite samples reached 99% and showed an equilibrium swelling ratio of less than 3%. The high gel fraction and low swelling ratios are consistent with successful uniform curing of pDCPD to form densely crosslinked and rigid networks during HAPPI AM.

Table 1 Gel fraction and equilibrium swelling ratio of pDCPD, pDCPD-CF, and pDCPD-fCF composite parts in ethanol, produced via HAPPI AM. Data collected from dogbone specimens

	Gel fraction in ethanol (%)	Equilibrium swelling ratio in ethanol (%)
DCPD	99.1 ± 0.3	3.1 ± 0.5
pDCPD+5%CF	99.9 ± 0.1	3.7 ± 0.4
pDCPD+10%CF	99.9 ± 0.1	1.5 ± 0.1
pDCPD+5%fCF	99.9 ± 0.1	3.2 ± 0.2
pDCPD+10%fCF	99.4 ± 0.1	2.2 ± 0.3

3.2 Mechanical performance of pDCPD and pDCPD-CF composites prepared by HAPPI AM and molding

To evaluate mechanical properties of the HAPPI AM parts derived from DCPD or DCPD with CFs or fCFs, we prepared dogbone samples using the resin formulations. The dimensional accuracy of representative printed dogbones were measured and we found an average length of

View Article Online
DOI: 10.1039/D5MA01441G

116.9 ± 0.2 mm (2% greater than the digital model, 114.4 mm), width of narrow gauge section of 9.5 ± 0.4 mm (24% greater than the model, 7.6 mm), and thickness of 2.9 ± 0.2 mm (7% less than the model, 3.2 mm). The significant increase (24%) in width of the narrow gauge section compared to the digital model is attributed to overgrowth during printing. For comparison, we also evaluated the results from molded samples cured by FROMP. We note that whereas HAPPI AM of DCPD alone was best conducted using 0.4 wt% of the PMPs, we found that HAPPI AM with additives in the formulation benefited from increased loadings of the PMPs. In general, the adjustments to the resin formulations were done empirically and were straightforward to enable versatility in the range of additives that can be used. We found that including oligoDCPD in the resin feed produced parts that were largely indistinguishable from those without the additive, based upon tensile testing results. Therefore, we discontinued the study of oligoDCPD. Incorporation of pTD-NB led to dogbone specimens that were too weak for tensile testing, and thus we also discontinued our studies of those formulations. Refocusing on the composite materials, we next examined the effect of CF and fCF on the mechanical properties of samples prepared by HAPPI AM versus molding. Tensile test results are summarized in Table 2 and depicted in Fig. 4 (uniaxial tensile testing stress-strain curves) and Fig. 5 (graphical data summary). In Fig. 4, the solid versus dashed lines of the same color compare HAPPI versus molded parts. Other notable pairs include blue versus green lines (5% CF versus 5% fCF) and orange versus red lines (10% CF versus 10% fCF). Incorporation of CF or fCF into the pDCPD matrix resulted in increased Young's modulus and ultimate strength in HAPPI samples, with maximum observed increases of 220% (from 1.1 to 2.5 GPa) and 170% (from 19.4 to 34.2 MPa), respectively. Molded samples also showed increased Young's modulus with the addition of CF or fCF by up to 220% (from 1.7 to 3.7 GPa), whereas the ultimate strength of molded samples was reduced with the addition of CF or fCF. Henderson and co-workers[35] also observed an increase in Young's modulus (from 1.7 to 2.7 to 3.2 GPa with 5, 10, or 15 wt% CF loading, respectively) and a decrease in the elongation at break across the same series. With CF or fCF, we observed ultimate strength values clustered near 50 MPa for molded dogbone samples regardless of CF loadings. This is consistent with previous studies that also report consistent ultimate strength (ca. 50 MPa) for neat pDCPD and pDCPD-CF composites at 5 to 10 wt% CF loading.[35] Leguizamon and co-workers found that molded pDCPD samples prepared by FROMP using PMPs showed a Young's modulus of 1.6 GPa, ultimate strength of 40 MPa, and elongation at break above 20%.[3] Those values are comparable with those of the molded samples in this study, except for the longer elongation at break, which might be attributed to the lower strain rate (3%·min^{-1} for ASTM type V) used in tensile tests. We also point out that although we are comparing our experimental results to literature values, slight differences in methodology can often have a significant impact on values for Young's modulus and strain at break.

View Article Online
DOI: 10.1039/D5MA01441G

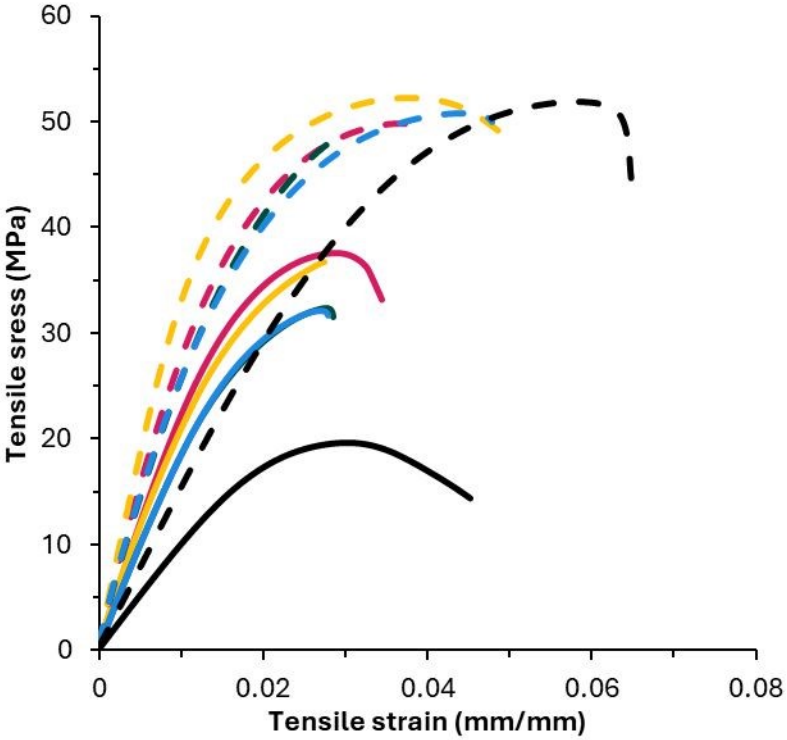

Fig. 4 Tensile test results on dogbone samples of pDCPD (●), pDCPD-5%CF (●), pDCPD-5%fCF (●), pDCPD-10%CF (●), and pDCPD-10%fCF (●) prepared by HAPPI AM (solid lines) and molding (dashed lines).

Table 2 Comparison between samples of pDCPD, pDCPD+5% CF, pDCPD+5%fCF, pDCPD+10%CF, and pDCPD+10% fCF prepared by HAPPI versus molding shown in Fig. 4. Values represent the average of three experiments; errors represent one standard deviation

Formulation	Young's modulus (GPa)		Ultimate strength (MPa)		ε at break (%)	
	HAPPI	Molded	HAPPI	Molded	HAPPI	Molded
DCPD	1.16 ±0.05	1.7 ±0.08	19.4 ±1.3	50.1 ±1.33	3.6 ±0.7	6.4 ±0.3
pDCPD+5%CF	2.37 ±0.32	3.48 ±0.28	29.3 ±2.3	51.1 ±0.25	3.1 ±0.7	4.3 ±1.1
pDCPD+5%fCF	2.07 ±0.09	2.72 ±0.47	27.5 ±3.9	48.8 ±2.56	3.5 ±1.6	3.9 ±1.6
pDCPD+10%CF	2.42 ±0.32	3.75 ±0.16	33.8 ±2.2	51.6 ±1.38	2.4 ±0.5	4.5 ±0.4

View Article Online
DOI: 10.1039/D5MA01441G

pDCPD+10%fCF	2.56 ±0.18	3.63 ±0.16	34.2 ±2.4	48.5 ±1.62	3.0 ±0.5	3.4 ±0.3

As can be seen in Fig. 4, composite samples prepared by HAPPI were generally consistent with one another, as were molded parts. This held true across Young's modulus, ultimate strength, and elongation at break regardless of loading (5 or 10 wt%) or surface functionalization of the fiber (CF vs. fCF). In this study, it seems the effect of CF on the mechanical properties would not be significant at concentrations above 5 wt% in the samples prepared by HAPPI or molding. Our tensile testing results further suggest that the pDCDP-fCF composites in this study were fractured during the loading before force was fully transferred to any fCF that could be covalently bonded (i.e., as depicted in Fig. 4) to the pDCPD matrix. We next compared the tensile properties of HAPPI samples to those of molded samples. Young's modulus and ultimate strength of HAPPI samples reached about 60 and 65% of values obtained for molded samples, respectively. Elongation at break of HAPPI samples reached about 55 to 85% of the values obtained from molded samples. We considered that over-curing of each layer during printing could occur and that it may lead to reduced mechanical properties compared to those of the molded samples. We further speculated that the reduced elongation at break for the HAPPI samples could have resulted from pores or defects formed during the HAPPI AM process and incomplete FROMP within the part. This hypothesis was explored further via SEM and CT scanning (see below). We further investigated mechanical properties of rectangles prepared from HAPPI or molding by DMA providing storage modulus (E') indicating the solid-like character of the samples, loss modulus (E") indicating liquid-like character, and tan (δ) as the ratio of E" to E'. Glass transition temperature (T_g) was determined at the peak of tan (δ). E' and tan (δ) of the samples are shown in Figs. S16 through S19, and E' at 33 °C (glassy state) and T_g from the tan (δ) peak were summarized in Table S2 and Fig. S20. We observed similar trends of E' with Young's modulus shown in Figs. 5 and 6. Incorporation of CFs or fCFs into the pDCPD resulted in increased E' in HAPPI and molded sample, with maximum observed increases of 205% and 151%, respectively though the effect of functionalization of CFs on E' was not significant. Additionally, the effect of CFs or CFs on T_g of pDCPD composites was more significant in HAPPI samples than in molded ones. Incorporation of CFs or fCFs in pDCPD increased T_g by maximum 47 °C (from 89 to 137 °C) in HAPPI samples while T_g of molded pDCPD or pDCPD-CF composites ranged between 150 °C and 161 °C.

View Article Online
DOI: 10.1039/D5MA01441G

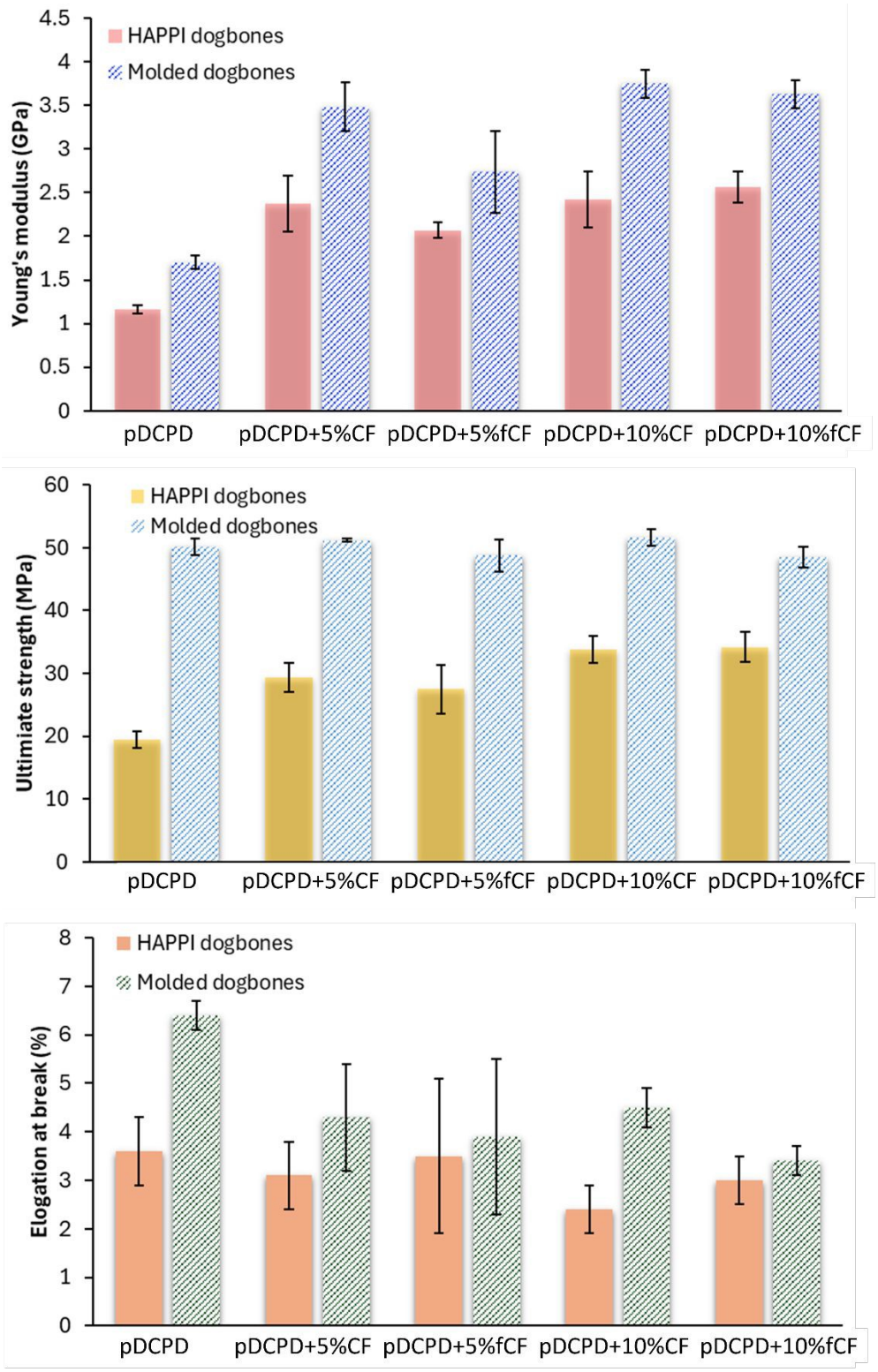

Fig. 5 Comparison of Young's modulus, ultimate strength, and elongation at break of dogbone samples prepared by HAPPI AM to those by molding shown in Table 2.

View Article Online
DOI: 10.1039/D5MA01441G

3.3 Microstructures of printed pDCPD and pDCPD-CF composites studied by SEM and CT scans

We examined fracture surfaces of the four sets of pDCPD-(f)CF composites by SEM to study the dispersion of CF or fCF in the pDCPD matrix and the interfaces between CF and pDCPD. Those two factors are important for transferring mechanical load across the fiber-matrix interfaces, which can strongly influence the mechanical performance of the composites.[32] Fig. 6 shows SEM images on fractured composites after tensile tests of (A) pDCPD-5%CF, (B) pDCPD-10%CF, (C) pDCPD-5%fCF, and (D) pDCPD-10%fCF. When Figs. 7(A) and 7(B) were compared to 7(C) and 7(D), we found that fCF were more uniformly dispersed in the pDCPD matrix than CF at both 5 wt% and 10 wt% loadings. The better dispersion of the fibers suggests that norbornene-functionalized CF are chemically more compatible with DCPD in the resin due to their having the same cycloolefin structures on the surface, in contrast with non-functionalized CF. We did not observe distinct interfaces between pDCPD-CF versus and pDCPD-fCF materials. We hypothesize that dogbones made via HAPPI AM underwent fracture during tensile tests before mechanical loads were fully transferred to the interfaces between the fibers and matrix. Therefore, the mechanical performance of pDCPD-fCF was similar to that of pDCPD-CF.

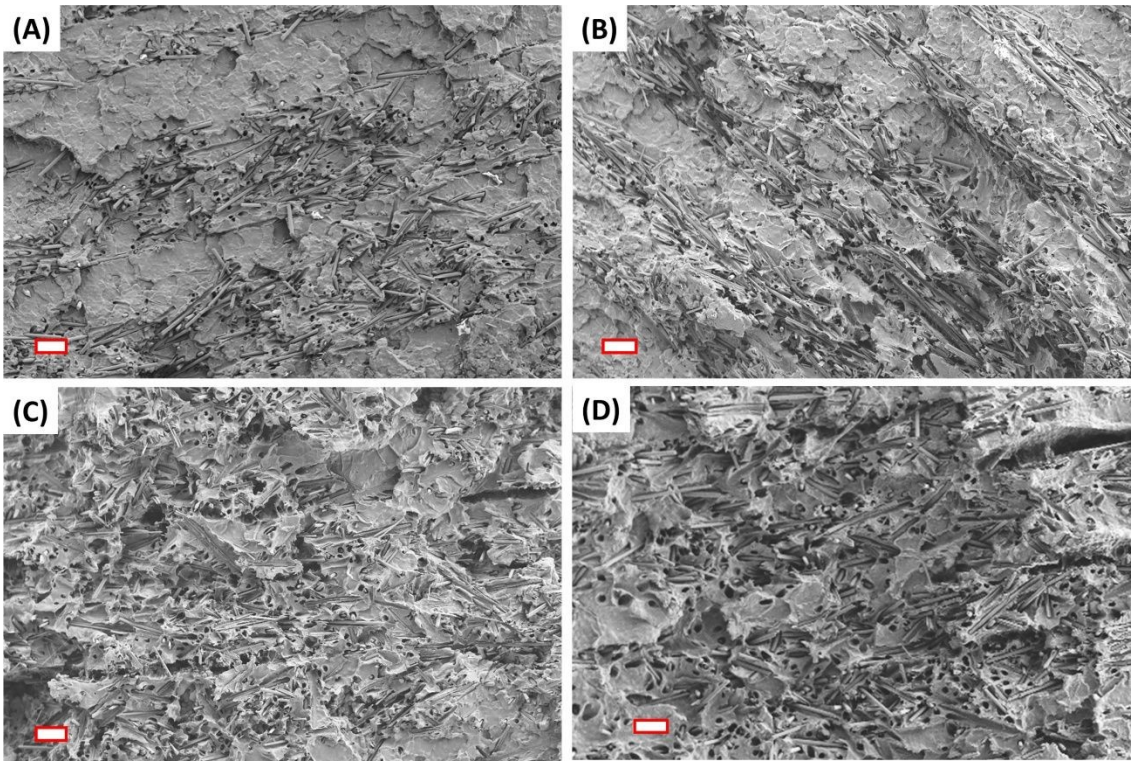

Fig. 6 SEM images on fracture surface of (A) pDCPD +5%CF, (B) pDCPD+10%CF, (C) pDCPD+5%fCF, and (D) pDCPD+10%fCF (scale bar = 100 μm).

View Article Online
DOI: 10.1039/D5MA01441G

To better understand the internal structures of the parts, we examined the microstructures of HAPPI printed pDCPD and pDCPD-(f)CF composites by CT imaging (Fig. 7). Fig. 7(A) shows one of the representative CT-scans in the fractured area of a pDCPD dogbone sample after a tensile test. It shows internal pores with irregular shapes along the printed layers. The porosity of representative samples was found to be 8.3 ± 0.7% according to our analysis using ImageJ. In comparison, molded samples were found to have an average porosity of 0.21 ± 0.09%, much denser than the HAPPI specimens. We suspect that the higher porosity in the HAPPI samples may result from the evaporation of DCPD during the printing process. This evaporation occurs across the layer surface and remains trapped at the interface as subsequent layers are printed. For the HAPPI samples, the Feret's diameter (or maximum pore length) of 577 pores was calculated by ImageJ, giving an average of 74 ± 70 μm, minimum of 10 μm, and maximum of 647 μm. Figs. 8(B) through 8(E) show CT scans of pDPCD-composites, with the CFs presenting as brighter features than pDCPD matrices. When Fig. 7(B) was compared with 8(C), we found that the 5 wt% CF sample had fibers that were more uniformly dispersed in pDCPD matrix than for the sample prepared with 10 wt% CF. When 8(B) and 8(C) were compared with 8(D) and 8(E), respectively, fCF were found to be more uniformly dispersed than non-functionalized CF, which is consistent with the results from SEM analysis (cf. Fig. 6). When 8(D) was compared with 8(E), we did not observe much difference in dispersion between 5 wt% fCF and 10 wt% fCF samples. Although we do note that the 5.3-micron resolution of the CT scans makes assessment of the dispersion difficult, our observations here are consistent with the SEM images and the saturated mechanical properties of the composites at 5 wt% CF (cf. Figs. 5 and 6).

We note that in our work, fibers in the pDCPD matrix are randomly oriented as shown via SEM in Fig. 6. and CT scans Fig. 7, meaning some full length of fibers are shown in those images. Additionally, CT analysis shows 2-dimensional slices, but the fibers will likely be tilted in 3D, making it difficult to get accurate lengths from this analysis. This point would lead to inaccurate measurement of fiber length and their distribution. We further note that fiber shortening after mechanical agitation was reported by Zhang et al.[23] In their studies, the length of as-received CF was 458 ± 400 μm and that of surface-modified CF was 84 ± 35 μm.

View Article Online
DOI: 10.1039/D5MA01441G

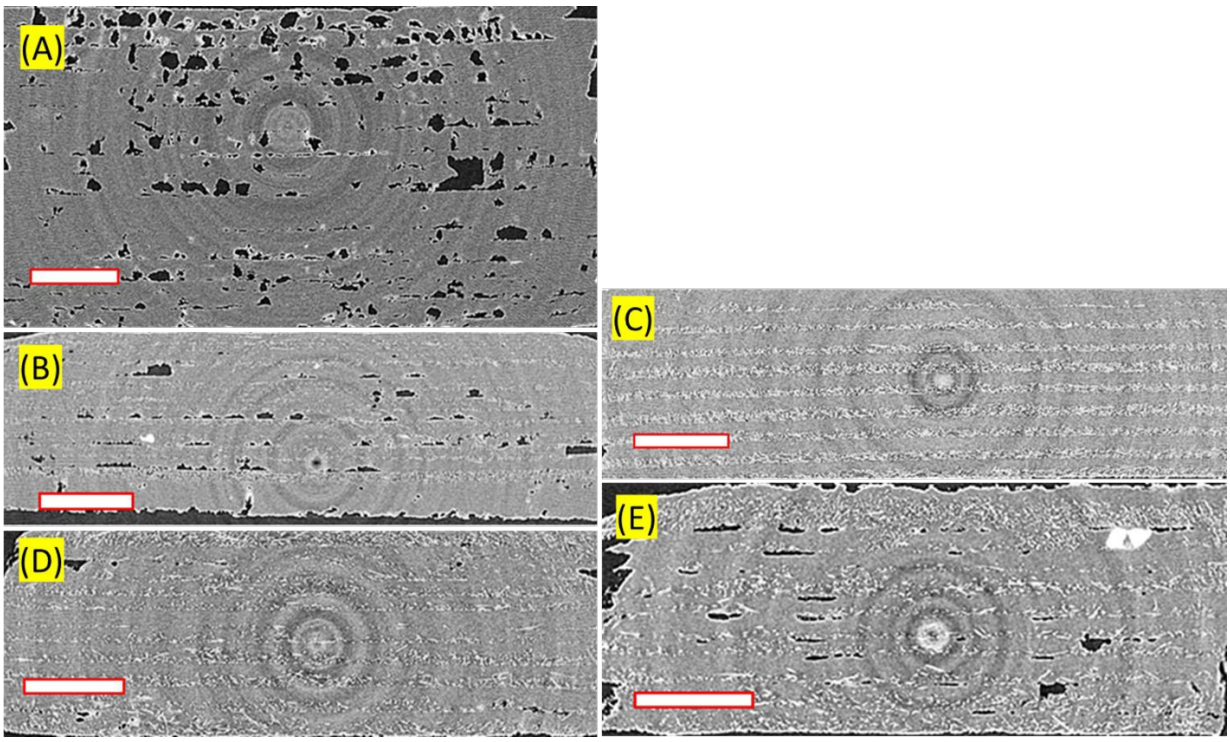

Fig. 7 CT-scans of (A) pDCPD, (B) pDCPD+5%CF, (C) pDCPD+10%CF, (D) pDCPD+5%fCF, and (E) pDCPD+10%fCF. (scale bar = 1 mm)

Conclusions

We demonstrated a new method to create three dimensional objects of pDCPD and pDCPD-CF composites with complex structures and via HAPPI AM, taking advantage of geometric freedom in a vat-type AM and irrelevance of optical properties of the resin. HG2-PSU PMPs designed for FROMP were used as thermo-responsive catalytic particles to initiate ROMP of pDCPD. Control of key parameters such as print conditions and temperature lead to localized heating followed by ROMP of pDCPD to create complex three-dimensional structures via layer-by-layer construction. More specifically, we empirically obtained the following serviceable HAPPI AM conditions: (1) reduced concentration of PMPs to 0.4 wt%, (2) limited thickness of the layers in HAPPI to 0.3 mm, (3) aging PMPs in DCPD for 4 to 7 days, and (4) controlled temperature of the photothermal plate between 150 to 200 ˚C while printing by manipulating the laser raster speed and laser power. Incorporating CF in the pDCPD matrices enhanced Young's modulus and ultimate strength in HAPPI samples, with maximum observed increases of 220% and 170%, respectively, although we did not observe significant effect of CF functionalization on the mechanical properties of the composites. Looking ahead, despite resolution limits in the HAPPI process, we envision HAPPI AM to enable pathways to create 3D composite structures of other thermosets, such as urethanes, thiol-ene networks, and thiol-epoxide materials.

Author contributions

View Article Online
DOI: 10.1039/D5MA01441G

SCL, CUL, AJB: conceptualization. SGF, AMK: investigation. SCL, LH, AJB: supervision. CUL: writing—original draft. All authors: methodology, writing—review & editing.

Conflicts of interest

The authors declare no competing interest.

Data availability

The data supporting this article have been included as part of the Supplementary Information. Supplementary information: Synthesis of poly(tetracyclododecene)-imide-norbornene (pTD-NB) – experimental details, NMR spectra, GPC data; DSC thermograms of DCPD with PSU-PMPs and PSU-PMPs and CF; videos and still images showing CT-scans of gyroid and spiral in Fig. 3.

Acknowledgements

This work was supported by the Laboratory Directed Research and Development Program (Project# 229367) at Sandia National Laboratories, a multimission laboratory managed and operated by the National Technology and Engineering Solutions of Sandia, LLC, a wholly owned subsidiary of Honeywell International Inc., for the U.S. Department of Energy's National Nuclear Security Administration under contract DE-NA-0003525. A.J.B. acknowledges partial financial support from the Yamamoto Family, the Office of the Vice Chancellor for Research and Graduate Education at the University of Wisconsin-Madison with funding from the Wisconsin Alumni Research Foundation, as well as the Army Research Office (W911NF-20-2-0182-P00005-(76555-EG-MUR)) and Office of Naval Research (N00014-23-1-2499). The authors gratefully acknowledge the use of facilities and instrumentation at the UW-Madison Wisconsin Centers for Nanoscale Technology (wcnt.wisc.edu) partially supported by the NSF through the University of Wisconsin Materials Research Science and Engineering Center (DMR-1720415). Any opinion, findings, conclusions, or recommendations expressed in this material are those of the authors(s) and do not necessarily reflect the views of any funding agency or sponsor.

References

1 S. Kovačič and C. Slugovc, *Mater. Chem. Front.*, 2020, **4**, 2235–2255.

2 J. C. Mol, *J. Mol. Catal. A Chem.*, 2004, **213**, 39–45.

3 O. Davydovich, A. J. Greenlee, H. D. Root, A. L. Jansen, S. C. Gallegos, M. J. Warner, M. S. Kent, J. A. Cardenas, L. N. Appelhans, D. J. Roach, B. H. Jones and S. C. Leguizamon, *Macromolecules*, 2023, **56**, 7543–7550.

4 S. C. Leguizamon, N. T. Monk, M. T. Hochrein, E. M. Zapien, A. Yoon, J. C. Foster and L. N. Appelhans, *Macromolecules*, 2022, **55**, 8273–8282.

5 O. Eivgi, R. S. Phatake, N. B. Nechmad and N. G. Lemcoff, *Acc. Chem. Res.*, 2020, **53**, 2456–2471.

View Article Online
DOI: 10.1039/D5MA01441G

6 O. Eivgi, A. Vaisman, N. B. Nechmad, M. Baranov and N. G. Lemcoff, *ACS Catal.*, 2020, **10**, 2033–2038.

7 J. C. Foster, A. W. Cook, N. T. Monk, B. H. Jones, L. N. Appelhans, E. M. Redline and S. C. Leguizamon, *Advanced Science*, 2022, **9**, 1–8.

8 S. C. Leguizamon, A. W. Cook and L. N. Appelhans, *Chemistry of Materials*, 2021, **33**, 9677–9689.

9 A. Balasubramanian and R. A. Weitekamp, US11,725,077B2, 2023.

10 R. A. Weitekamp, R. H. Grubbs, H. A. Atwater and J. Fakonas, US Pat., 10799613B2, 2020.

11 I. D. Robertson, L. M. Dean, G. E. Rudebusch, N. R. Sottos, S. R. White and J. S. Moore, *ACS Macro Lett.*, 2017, **6**, 609–612.

12 D. G. Ivanoff, J. Sung, S. M. Butikofer, J. S. Moore and N. R. Sottos, *Macromolecules*, 2020, **53**, 8360–8366.

13 B. A. Suslick, J. Hemmer, B. R. Groce, K. J. Stawiasz, P. H. Geubelle, G. Malucelli, A. Mariani, J. S. Moore, J. A. Pojman and N. R. Sottos, *Chem. Rev.*, 2023, **123**, 3237–3298.

14 I. D. Robertson, M. Yourdkhani, P. J. Centellas, J. E. Aw, D. G. Ivanoff, E. Goli, E. M. Lloyd, L. M. Dean, N. R. Sottos, P. H. Geubelle, J. S. Moore and S. R. White, *Nature*, 2018, **557**, 223–227.

15 V. Alzari, D. Nuvoli, D. Sanna, A. Ruiu and A. Mariani, *J. Polym. Sci. A Polym. Chem.*, 2016, **54**, 63–68.

16 C. U. Lee, K. C. H. Chin and A. J. Boydston, *ACS Appl. Mater. Interfaces*, 2023, **15**, 16072–16078.

17 A. Boydston and C.-U. Lee, US Pat., 11597145 B2, 2023.

18 C. U. Lee, S. J. Kim, R. B. Dietrich, A. L. Girard and A. J. Boydston, *Green Chemistry*, 2024, **26**, 9814–9822.

19 A. L. Cook, M. A. Dearborn, T. M. Anderberg, K. Vaidya, J. E. Jureller, A. P. Esser-Kahn and A. H. Squires, *ACS Appl. Mater. Interfaces*, 2024, **16**, 17973–17980.

20 J. E. Aw, X. Zhang, A. Z. Nelson, L. M. Dean, M. Yourdkhani, R. H. Ewoldt, P. H. Geubelle and N. R. Sottos, *Adv. Mater. Technol.*, DOI:10.1002/admt.202200230.

21 M. Ziaee, J. W. Johnson and M. Yourdkhani, *ACS Appl. Mater. Interfaces*, 2022, **14**, 16694–16702.

View Article Online
DOI: 10.1039/D5MA01441G

22 C. F. Dojan, M. Ziaee, A. Masoumipour, S. J. Radosevich and M. Yourdkhani, *Nat Commun*, 2025, **16**, 1–10.

23 S. Huang, Z. Chen, Z. Feng, H. Zhao, L. Ye, L. Weng, Z. Xie, S. Liu, D. Jiang and W. Chen, *Adv. Mater*, 2025, **15033**, 1–13.

24 M. Yourdkhani, A. Masoumipour, M. Ziaee, S. Dashtizad and C. F. Dojan, *npj Advanced Manufacturing*, DOI:10.1038/s44334-025-00062-9.

25 Y. B. Lee, Y. S. Kim, C. Chen, M. T. Hossain, B. A. Suslick, R. H. Ewoldt, S. H. Tawfick, J. S. Moore, N. R. Sottos and P. V. Braun, *Adv. Mater*, DOI:10.1002/adma.202508568.

26 Z. Zhang, R. Liu, W. Li, Y. Liu, Z. Pei, J. Qiu and S. Wang, *J. Manuf. Process.*, 2021, **71**, 753–762.

27 N. S. Hmeidat, M. Zakoworotny, Y. S. Kim, T. B. Le, G. DeBrun, R. Shah, J. J. Lessard, J. S. Moore, J. W. Baur, P. H. Geubelle, N. R. Sottos and S. H. Tawfick, *Compos. Part A Appl. Sci. Manuf.*, 2025, **190**, 108609.

28 L. M. Dean, A. Ravindra, A. X. Guo, M. Yourdkhani and N. R. Sottos, *ACS Appl. Polym. Mater.*, 2020, **2**, 4690–4696.

29 S. Asif, P. Chansoria and R. Shirwaiker, *J. Manuf. Process.*, 2020, **56**, 1340–1343.

30 L. Wang, H. Wu, A. Guo, D. Kong, Z. Zhao, C. Liu, L. Yin, G. Xia, X. Su, Z. Chen and D. Wang, *Materials*, 2024, **17**, 3127. DOI:10.3390/ma17133127.

31 Y. Lu, X. Han, A. Gleadall, F. Chen, W. Zhu and L. Zhao, *Addit. Manuf.*, 2022, **60**, 103233.

32 D. J. Hayne, M. Singleton, B. A. Patterson, D. B. Knorr, F. Stojcevski and L. C. Henderson, *Compos. Commun.,* 2024, **47**, 101872.

33 T. Tian, J. Wang, S. Wu, Z. Shao, T. Xiang and S. Zhou, *Polym. Chem.*, 2019, **10**, 3488–3496.

34 C. Unterweger, O. Bruggemann and C. Furst, *Polym. Compos.*, 2014, **35**, 227–236.

35 D. J. Hayne, M. A. Singleton, B. A. Patterson, Y. Athulya Wickramasingha, J. M. Sietins, D. B. Knorr, F. Stojcevski and L. C. Henderson, *Compos. Part A Appl. Sci. Manuf.*, 2022, **155**, 106839.

36 Y. S. Kim, M. Zhu, M. T. Hossain, D. Sanders, R. Shah, Y. Gao, J. S. Moore, N. R. Sottos, R. H. Ewoldt, P. H. Geubelle and S. H. Tawfick, *Adv. Mater*, DOI:10.1002/adma.202406265.

View Article Online
DOI: 10.1039/D5MA01441G

Data availability statements

The data supporting this article have been included as part of the Supplementary Information. Supplementary information: Synthesis of poly(tetracyclododecene)-imide-norbornene (pTD-NB) – experimental details, NMR spectra, GPC data; DSC thermograms of DCPD with PSU-PMPs and PSU-PMPs and CF; videos and still images showing CT-scans of gyroid and spiral in Fig. 3.